Earth, Planets and Space

FULL PAPER Open Access

Continuous monitoring of soil CO_2 flux at Aso volcano, Japan: the influence of environmental parameters on diffuse degassing

Masaaki Morita[1*], Toshiya Mori[2], Akihiko Yokoo[3], Takahiro Ohkura[3] and Yuichi Morita[4]

Abstract

Continuous measurements of soil CO_2 flux are useful for understanding degassing processes and for monitoring volcanic activities. Recent studies at many volcanoes have revealed that soil CO_2 flux variations are significantly influenced by environmental parameters as well as volcanic processes. In this study, we conducted continuous monitoring of soil CO_2 flux in the flank of Nakadake cone, Aso volcano, Japan, from January 2016 to November 2017. The results of our observations during an active period before and after a large phreatomagmatic eruption on 8 October 2016 and during a calm period from 2017 showed variations in soil CO_2 flux due to oscillations in environmental parameters. Excluding these variations from the raw time series by multivariate linear regression analysis, the time series of soil CO_2 flux presented some anomalous peaks in both the active and calm periods. Careful comparison of the anomalous peaks with the environmental parameters revealed that most of the anomalous peaks were likely due to an increase in wind speed and/or a decrease in barometric pressure. However, the anomaly after the 8 October 2016 eruption was not completely explicable by the variations in the environmental parameters and coincided with increases in seismic amplitude and plume SO_2 flux. This anomaly was possibly attributed to an increase in magmatic CO_2 flux. These findings emphasized the importance of careful statistical treatment of the soil CO_2 flux data after excluding the influences of the environmental parameters at each measurement site. These statistical treatments will contribute to a better understanding of the degassing processes and monitoring of volcanic activities, including phreatic or phreatomagmatic eruptions.

Keywords: Aso volcano, Soil CO_2 flux, Accumulation chamber method, Multiple linear regression analysis, Environmental parameters

Introduction

Soil diffuse degassing is an important part of gas emissions from active volcanoes and hydrothermal systems (Baubron et al. 1990; Allard et al. 1991). Among the many species in magmatic gases, CO_2 is a good indicator of the migration of magmatic volatiles because of its high abundance in magmatic volatiles and its low solubility in magma (Stolper and Holloway 1988). Associated with volcanic unrests, anomalous increases in soil CO_2 fluxes have been reported at many volcanoes (Rogie et al. 2001; Hernández et al. 2001; Granieri et al. 2003; Carapezza et al. 2004; Badalamenti et al. 2004; Carapezza et al. 2009; Pérez et al. 2012; Werner et al. 2014; Laiolo et al. 2016; Cardellini et al. 2017; Boudoire et al. 2017). These anomalous increases have been detected as precursory changes measured by automated monitoring systems (e.g., Pérez et al. 2012; Boudoire et al. 2017) and/or as an expansion in anomalous degassing areas and an increase in background CO_2 flux measured by repeated spatial surveys of soil CO_2 flux (e.g., Cardellini et al. 2017). For example,

*Correspondence: aki.morita@aist.go.jp
[1] Geological Survey of Japan, National Institute of Advanced Industrial Science and Technology, Central 7, Higashi 1-1-1, Tsukuba, Ibaraki 305-8567, Japan
Full list of author information is available at the end of the article

based on continuous monitoring, large CO_2 flux anomalies have been recorded in coincidence with major explosions and lava flows at Stromboli volcano (Laiolo et al. 2016) and with the swarm of deep seismic events that preceded the eruption of Piton de la Fournaise volcano (Boudoire et al. 2017). These previous studies indicate that continuous measurements of soil CO_2 flux are useful for understanding degassing processes and for monitoring volcanic activities related to the migration of magma and volcanic gas from depth. The previous studies have conducted mainly at "dry" volcanoes where magmatic eruptions occurred, and there have not been any reports of soil CO_2 flux measurements related to phreatic or phreatomagmatic eruptions occurred at "wet" volcano.

Soil gas emissions, including those of CO_2, are significantly influenced by environmental parameters such as barometric pressure, air temperature, air humidity, soil temperature, soil humidity, rainfall, wind speed, and wind direction (Rogie et al. 2001; Granieri et al. 2003; Pérez et al. 2006; Lewicki et al. 2007; Viveiros et al. 2008; Carapezza et al. 2009; Cigolini et al. 2009; Liuzzo et al. 2013; Viveiros et al. 2014; Lewicki and Hilley 2014; Laiolo et al. 2016; Boudoire et al. 2017). To remove the contribution of these external parameters, Granieri et al. (2003) applied multiple regression analysis to time series of soil CO_2 flux for the first time. By using the same procedure, Viveiros et al. (2008) reported that the contribution of these environmental parameters to soil CO_2 flux variations reached more than 50% in their case. Among the environmental parameters, recent studies have revealed that soil conditions (soil temperature, soil humidity, and rainfall), as well as air temperature and barometric pressure, may highly influence soil CO_2 flux variations (Viveiros et al. 2008; Boudoire et al. 2017). Furthermore, soil CO_2 flux can be affected by local wind conditions around the monitoring site because of dynamic coupling between the wind and vadose zone of source CO_2 (Lewicki et al. 2007). The influence of each environmental parameter varies with site location (Viveiros et al. 2008; Carapezza et al. 2009); therefore, correlations between the environmental parameters and soil CO_2 flux at each monitoring site should be quantified to discriminate soil CO_2 flux variations related to changes in volcanic activity.

In the present study, continuous monitoring of soil CO_2 flux was performed at Aso volcano, Japan, starting in January 2016 following the volcanic unrest from the end of 2013 (Miyabuchi et al. 2018). Here, we present the results of the obtained data in 23 months including a large phreatomagmatic eruption on 8 October 2016. The environmental and volcanic influences on the data were distinguished using multiple linear regression (MLR) analysis. Our motivation was to evaluate the influence of the environmental parameters on our monitoring site of soil CO_2 flux and to validate the influence of the volcanic activity on the observed soil CO_2 flux. This study is the first investigation of soil degassing behavior during phreatic and phreatomagmatic eruptions.

Volcanic activities of Aso volcano during 2013–2017

Aso volcano is located on Kyushu Island, southwest Japan (Fig. 1). It consists of a caldera with diameters of 25 km in the north–south direction and 18 km in the east–west direction and post-caldera central cones. The only active cone is Nakadake volcano, which is a composite volcano of basalt to basaltic andesite (Ono and Watanabe 1985). Among the seven craters of the volcano, only the northernmost crater (the Nakadake first crater) has been active in the past 80 years (Ono and Watanabe 1985). During calm periods, the crater contains hot (40–80 °C) and hyper-acidic (pH < 1) lake water (Miyabuchi and Terada 2009; Ohsawa et al. 2010; Terada et al. 2012; Shinohara et al. 2015). Volcanic gases are persistently emitted from the lake surface and a fumarolic area on the southern wall of the crater (Fig. 1; Shinohara et al. 2015). The SO_2 flux in the calm periods typically ranges from 200 tons day^{-1} to 400 tons day^{-1} based on monthly reports by the Japan Meteorological Agency (JMA; available at http://www.data.jma.go.jp/svd/vois/data/tokyo/STOCK/monthly_vact_doc/monthly_vact_vol.php?id=503).

A timeline of the volcanic activity during 2013–2017 is summarized in Fig. 2. From April 2013, the surface area of the crater lake started to decrease, and it became less than 10% of the crater bottom in December 2013 (Fig. 2a; JMA 2015). Following multiple small ash emission events in January and February 2014 (Ichimura et al. 2018), the crater bottom was completely dried up in July 2014. A minor eruption occurred on 30 August, and a series of magmatic eruptions then began from 25 November (JMA 2015; Ichimura et al. 2018). Intermittent ash emissions and Strombolian explosions (referred to as "Strombolian eruptions" in Fig. 2a) at the vent situated in the crater (Fig. 1) continued until 3 May 2015 (Yokoo and Miyabuchi 2015; Miyabuchi et al. 2018). After the rainy season from the end of May to the middle of July, minor eruptions occurred from August 2015 (JMA 2016). An explosive phreatomagmatic eruption occurred on 14 September, in which the ash plume rose to 2000 m above the crater rim and 1-km running pyroclastic density currents were observed (Miyabuchi et al. 2018).

After the 14 September 2015 eruption, small phreatomagmatic explosions occurred on 23 October 2015, and some minor phreatic explosions occurred on 7 and 25 December 2015; 17 and 18 February 2016; and 4 March 2016 (Fig. 2a; JMA 2016, 2017). From March 2016, a small amount of hot water was observed in the

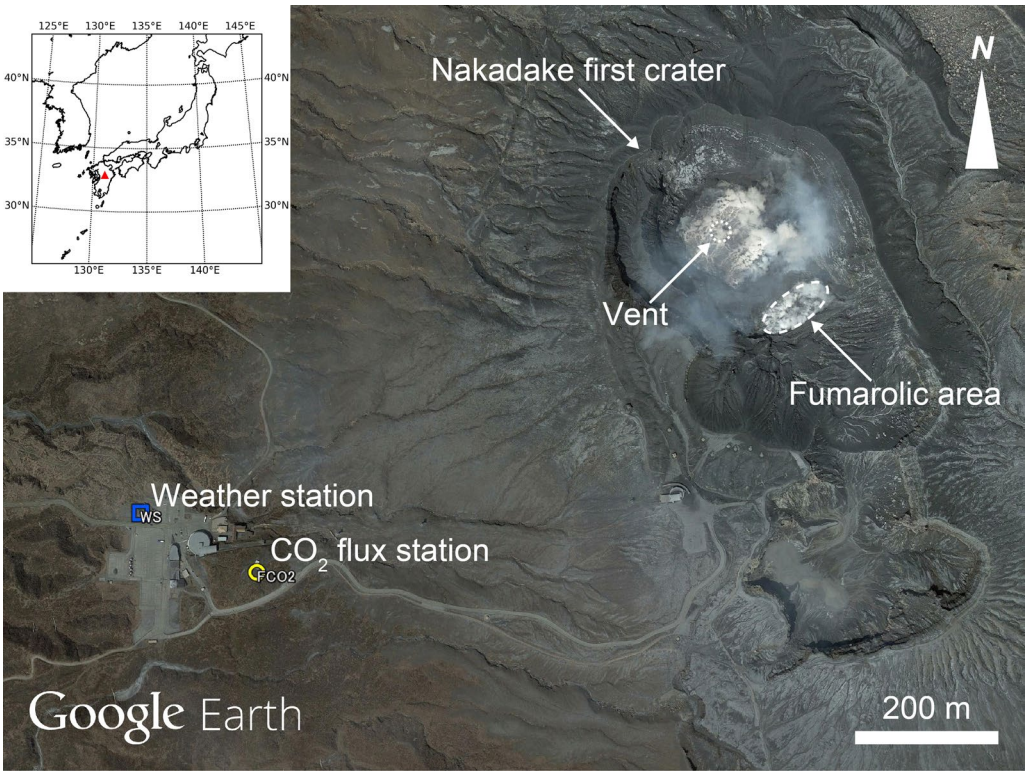

Fig. 1 Location of the soil CO_2 flux station (yellow circle) and weather station maintained by the Japan Meteorological Agency (blue square). The location of Aso volcano is depicted with a red triangle in an inset. The background satellite image (captured on 15 April 2016) is from Google Earth (https://earth.google.com/web/)

crater until the middle of July, and the surface area of the lake increased to 70% of the total area of the crater bottom (Fig. 2a; JMA 2017). During March and September 2016, quite minor mud emissions from the crater bottom were observed (JMA 2017). During this period, a large and destructive earthquake (Kumamoto earthquake, $M_w = 7.1$) occurred on 16 April 2016 at 40 km southwest of Aso volcano with many large ($M_{JMA} \leq 6.5$) foreshocks and aftershocks (Yagi et al. 2016).

On 8 October 2016, an explosive phreatomagmatic eruption occurred, and since then no eruptions have been recorded to this date (August 2018). The eruption plume height observed by the meteorological satellite Himawari-8 was estimated to reach 13–14 km asl (Ishii et al. 2018). After this eruption, bubbling in the lake water and a reddish glow around the fumarolic area in the southern crater wall were observed on 16 November (JMA 2017). The crater lake recovered and filled the crater bottom in April 2017 and has remained until the present (December 2018).

Continuous monitoring of soil CO_2 flux

Following the eruptions during 2014–2015, an automated soil CO_2 flux station (manufactured by West Systems Srl) was installed 1 km southwest of the active crater in January 2016 (Fig. 1). This location was selected because the volcano was very active during the installation and accessing the summit area during the automated measurements posed a high risk. In this location, a site was selected where the soil surface was devoid of any plants. Because a previous study of the spatial distribution of soil CO_2 flux was limited to the area in and around the Nakadake craters (Saito et al. 2007), any prior information about fluxes or the isotopic composition of soil CO_2 around the site was not available before we set the station at this site. The station stood on a volcanic edifice of the Nakadake cone consisting of layered lava flows and tuff (Ono and Watanabe 1985).

The station performed soil CO_2 flux measurements using the accumulation chamber method (Parkinson 1981; Chiodini et al. 1998). Every hour a chamber automatically descended into the ground, and the station

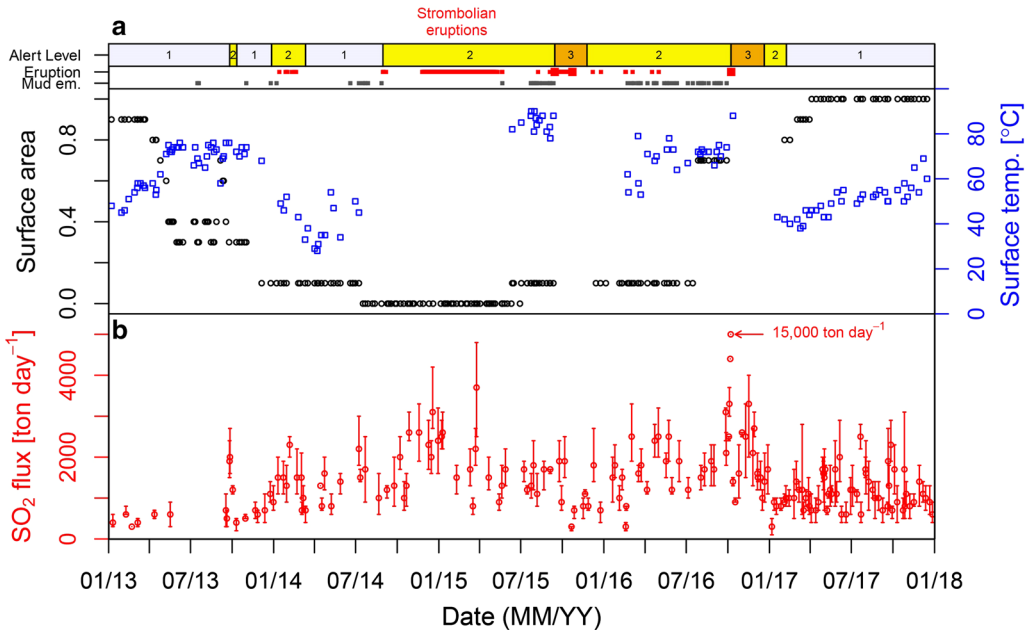

Fig. 2 Time series of **a** the surface area (black circle) and surface temperature (blue square) of the crater lake and **b** plume SO_2 flux. The surface area of the crater lake is indicated by the ratio of the area to the crater bottom. The value of 0 in the surface area corresponds to the situation where the crater lake does not exist. The value of 0.1 in the surface area includes the situation where although the crater lake exists, the amount of water cannot be estimated because the crater is mostly covered by the volcanic plume. At the upper part of **a**, volcanic alert levels issued by the Japan Meteorological Agency (JMA) are presented with a corresponding color code, and the dates of occurrence of eruptions and quite minor mud emissions from the crater bottom are depicted with red and gray dots, respectively. The enlarged dots of eruptions correspond to the phreatomagmatic eruptions on 14 September 2015, 23 October 2015, and 8 October 2016. The text "Strombolian eruptions" corresponds to the period when magmatic eruptions were observed (i.e., intermittent ash emissions and Strombolian eruptions). The data are from monthly reports by the JMA (available at http://www.data.jma.go.jp/svd/vois/data/tokyo/STOCK/monthly_v-act_doc/monthly_vact_vol.php?id=503)

measured soil CO_2 flux and environmental parameters, such as air temperature, air relative humidity, barometric pressure, wind speed, wind direction (direction where the wind blew from), soil humidity, soil temperature, and precipitation (Additional file 1: Table S1). Details of the measurement are described in the supplementary information (Additional file 1). Dionis et al. (2015) reported that the accuracy of the soil CO_2 flux measurement was within ± 25% for the range of 22–220 g m^{-2} day^{-1} using a similar instrument. Although a typical value of soil CO_2 flux in the present study was one order of magnitude lower than the range of soil CO_2 flux for the reported accuracy, the accuracy of the soil CO_2 flux in the present study unlikely deviated from the previous value, as shown in Additional file 1: Figure S1.

In the present study, the data collected between 8 January 2016 and 20 November 2017 were reported. The sensor for air temperature and air relative humidity malfunctioned during September–December 2016 and from August 2017 to the end of the present study. The rain gauge was also out of order from October 2016. Therefore, for air temperature and precipitation data of the missing period, the data obtained at a weather station maintained by the JMA (200 m from the soil CO_2 flux station; Fig. 1) were used. Detailed treatments of the missing data are described in the supplementary information (Additional file 1: Figure S2). For the air relative humidity data, the data from the weather station were used for the whole observation period in the analysis. The environmental parameters at the weather station were also missing during October 2016–January 2017 because of damage caused by the 8 October 2016 eruption. We linearly interpolated the air temperature data during this 3-month period. Furthermore, during the winter season (late December to March), our station was often covered with snow and the accumulation chamber system often froze. Consequently, soil CO_2 flux data in the winter season were frequently missing.

Results

A time series of soil CO_2 flux is shown in Fig. 2. The soil CO_2 flux ranged from 0.01 to 46.4 g m^{-2} day^{-1}, with a mean and a standard deviation of 2.1 g m^{-2} day^{-1} and 2.6 g m^{-2} day^{-1}, respectively (Fig. 3; Table 1). These flux values were one order of magnitude lower than the typical range of soil CO_2 flux in a volcanic-hydrothermal

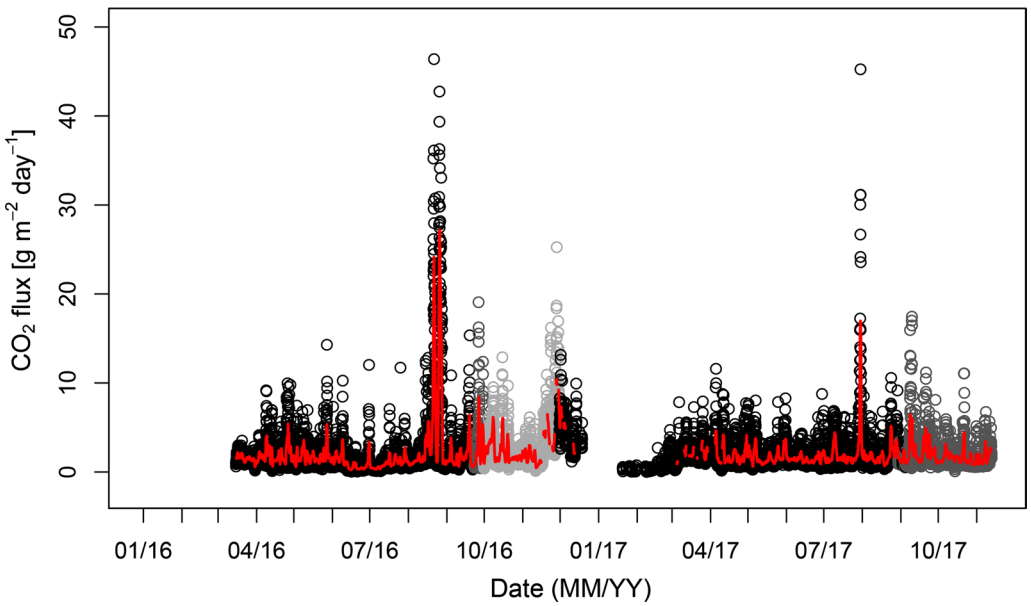

Fig. 3 Time series of soil CO_2 flux from January 2016 to November 2017 (black circle). The dark and light gray circles correspond to soil CO_2 flux data calculated with air temperature data of the weather station and interpolated air temperature data, respectively. The red line shows the daily average values of the data

Table 1 Statistics of soil CO_2 flux and environmental parameters

Parameter	Unit	Data no.	Mean	SD	Min.	Max.
Soil CO_2 flux	g m^{-2} day^{-1}	12,370	2.1	2.6	0.01	46.4
Barometric pressure	hPa	16,136	884.7	4.4	862.1	896.3
Air temperature	°C	14,899	11.8	8.8	−14.1	30.7
Air relative humidity	%	13,471	82.9	18.9	6.0	100.0
Precipitation	mm h^{-1}	14,293	0.5	2.3	0.0	75.2
Soil temperature	°C	16,136	12.4	7.3	0.4	23.4
Soil humidity	%	16,136	16.7	4.9	2.8	32.3
Wind speed	m s^{-1}	16,136	2.5	2.0	0.0	14.3
Wind direction	°North	16,136	nd	nd	0	359

SD Standard deviation, *nd* not determined

environment (Chiodini et al. 2008). However, even when the soil CO_2 flux was as low as the range observed in the present study, the contribution of magmatic CO_2 was observed in the time series of soil CO_2 flux (Pérez et al. 2012; Melián et al. 2014). In the present study, the station stood on bare ground, and there were no potential contributors to biogenic CO_2 around the station. Although we lacked data on the isotopic composition of the soil CO_2, a biogenic source of CO_2 alone did not unlikely explain the large variations (approximately 20 times larger than the average) in soil CO_2 flux observed in the present study.

As shown in Fig. 3, some high and low soil CO_2 flux trends were observed. Automated soil CO_2 flux measurement was not successfully performed from January to early March 2016 and from late December to early March 2017 because the accumulation chamber system often froze. However, during these winter seasons, the obtained soil CO_2 flux was as low as 0 g m^{-2} day^{-1} even when the measurement succeeded (Fig. 3). This low value was likely related to snow and soil frost, which made CO_2 not ascend in a shallow zone of the ground. The maximum soil CO_2 flux was observed in August 2016, and soil CO_2 flux at a comparable level was also found in August 2017 (Fig. 3). Soil CO_2 flux variations related to the Kumamoto earthquake (16 April 2016) were not evident. Minima in soil CO_2 flux occurred during June–July 2016, and a small increase in

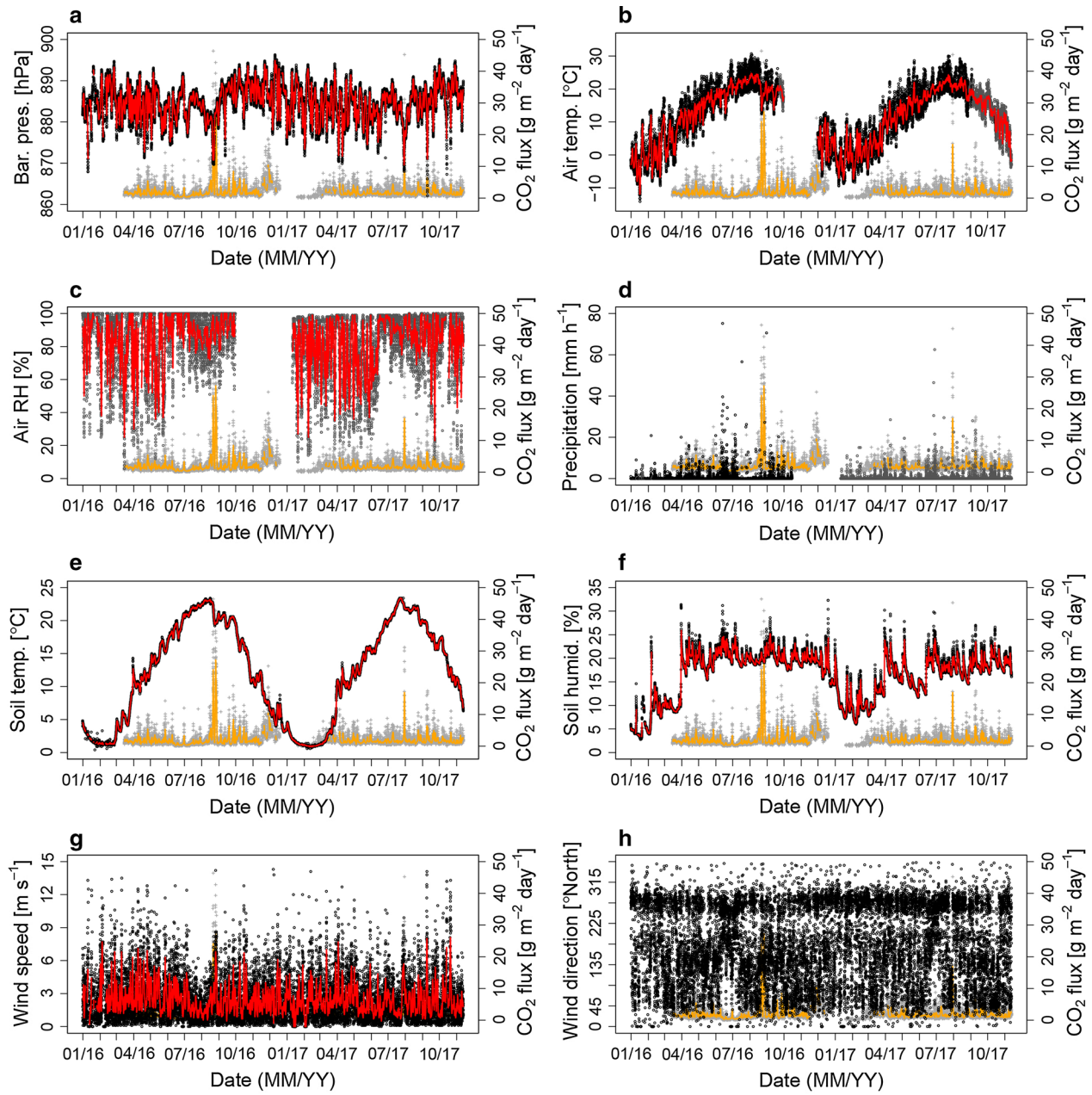

Fig. 4 Time series of environmental parameters from January 2016 to November 2017 for **a** barometric pressure, **b** air temperature, **c** air relative humidity, **d** precipitation, **e** soil temperature, **f** soil humidity, **g** wind speed, and **h** wind direction. The black and dark gray circles correspond to data obtained at the soil CO_2 flux station and those obtained at the weather station, respectively. The red line shows the daily average values of the data. The gray crosses and orange dotted line correspond to soil CO_2 flux and its daily average values shown in Fig. 3, respectively

the daily average values was recorded during November–December 2016.

A time series of environmental parameters is shown in Fig. 4, and the statistics are summarized in Table 1. By comparing the time series of environmental parameters with those of the soil CO_2 flux in Fig. 4, we recognized that the variations in soil CO_2 flux were often recorded simultaneously with increases or decreases in some of the environmental parameters. The increases in soil CO_2 flux in August 2016 and August 2017 were recorded simultaneously with decreases in barometric pressure or increases in wind speed (Fig. 4a, g). The minima in soil CO_2 flux during

June–July 2016 was observed during the rainy season with high precipitation and high soil humidity (Fig. 4d, f).

To clarify the statistical characteristics of the observed soil CO_2 flux and its correlation with the environmental parameters, a histogram and probability plot of the soil CO_2 flux and correlation plots of the daily average soil CO_2 flux and that of each parameter are shown in Fig. 5 and Additional file 1: Figure S3, respectively. As shown in Fig. 5, the soil CO_2 flux data roughly followed the lognormal distribution but were skewed right in the higher flux range; and thus, the soil CO_2 flux was plotted in logarithmic scale in Additional file 1: Figure S3. The correlation coefficients are summarized in Table 2. Among the eight environmental parameters, there was a relatively weak correlation between logarithmic soil CO_2 flux and wind speed (correlation coefficient $R = 0.414$), but the other parameters did not show significant correlations ($-0.3 < R < 0.3$). The lack of clear correlation between soil CO_2 flux and the environmental parameters did not agree with the results of previous studies (Viveiros et al. 2008; Carapezza et al. 2009; Laiolo et al. 2016). The lack of clear correlation may have been related to the differences between the present study and the previous studies in conditions of the site, including permeability and porosity of the soils, as well as the distance from the site to the hydrothermal system.

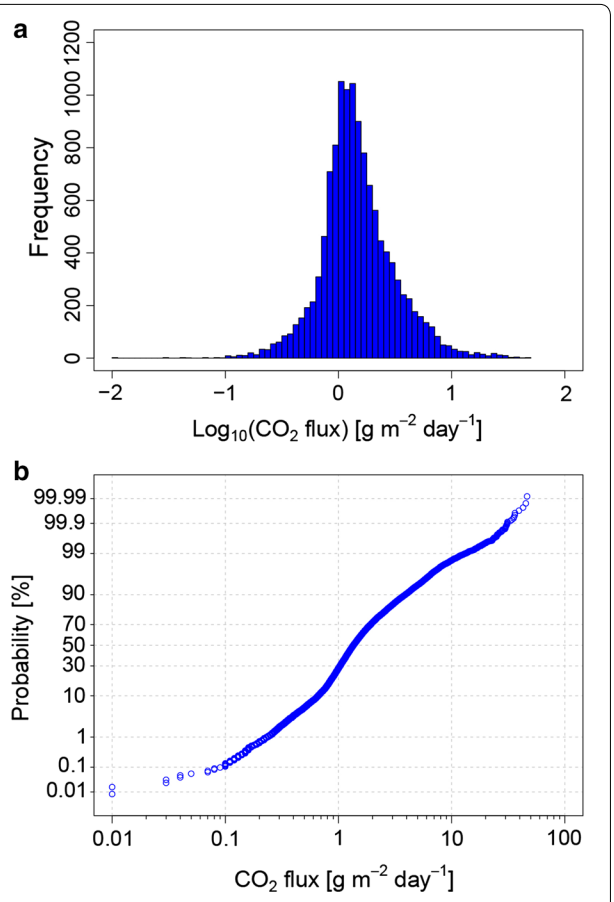

Fig. 5 **a** Histogram and **b** lognormal probability plot of soil CO_2 flux data

In Fig. 6, conditional probabilities (Carslaw 2015) of soil CO_2 flux ranging in the first, second, third, and fourth quartiles (< 0.95, 0.95–1.4, 1.4–2.2, and > 2.2 g m^{-2} day^{-1}, respectively) are plotted against wind speed and direction. For example, when the wind speed was 5 m s^{-1} and wind direction was northeast, the probability of soil CO_2 flux ranging in the third quartile was about 30% (Fig. 6c).

It is clear from Fig. 6a that soil CO_2 flux as low as the first quartile range (< 0.95 g m^{-2} day^{-1}) was recorded mainly with southwesterly wind. These azimuthal dependences were likely caused by the local terrain conditions of the soil CO_2 flux station. There was a small cliff of several meters height in the southwestern side of the station. The southwesterly winds might have caused air perturbation of the ascending CO_2 in the shallow part of the ground, thereby resulting in low soil CO_2 flux, as discussed in Lewicki et al. (2007). On the other hand, high soil CO_2 flux was observed principally in easterly wind conditions, and higher flux values were

Table 2 Correlation coefficient (*R*) between the daily average of log$_{10}$(soil CO_2 flux) and environmental parameters, 95% confidence interval of *R* (R_{95}), and *t* test and *p* values for *R*

Parameter	Degree of freedom	*R*	R_{95}	*t* test	*p* value
Barometric pressure	11,554	−0.145	−0.162 to −0.127	−15.71	0.00
Air temperature	11,554	−0.244	−0.261 to −0.226	−27.00	0.00
Air relative humidity	9847	−0.039	−0.059 to −0.019	−3.85	0.00
Precipitation	10,532	−0.077	−0.096 to −0.058	−7.91	0.00
Soil temperature	11,554	−0.125	−0.143 to −0.107	−13.51	0.00
Soil humidity	11,554	−0.124	−0.142 to −0.106	−13.48	0.00
Wind speed	11,554	0.414	0.399 to 0.429	48.86	0.00

The air temperature data used in this statistical treatment include the interpolated values

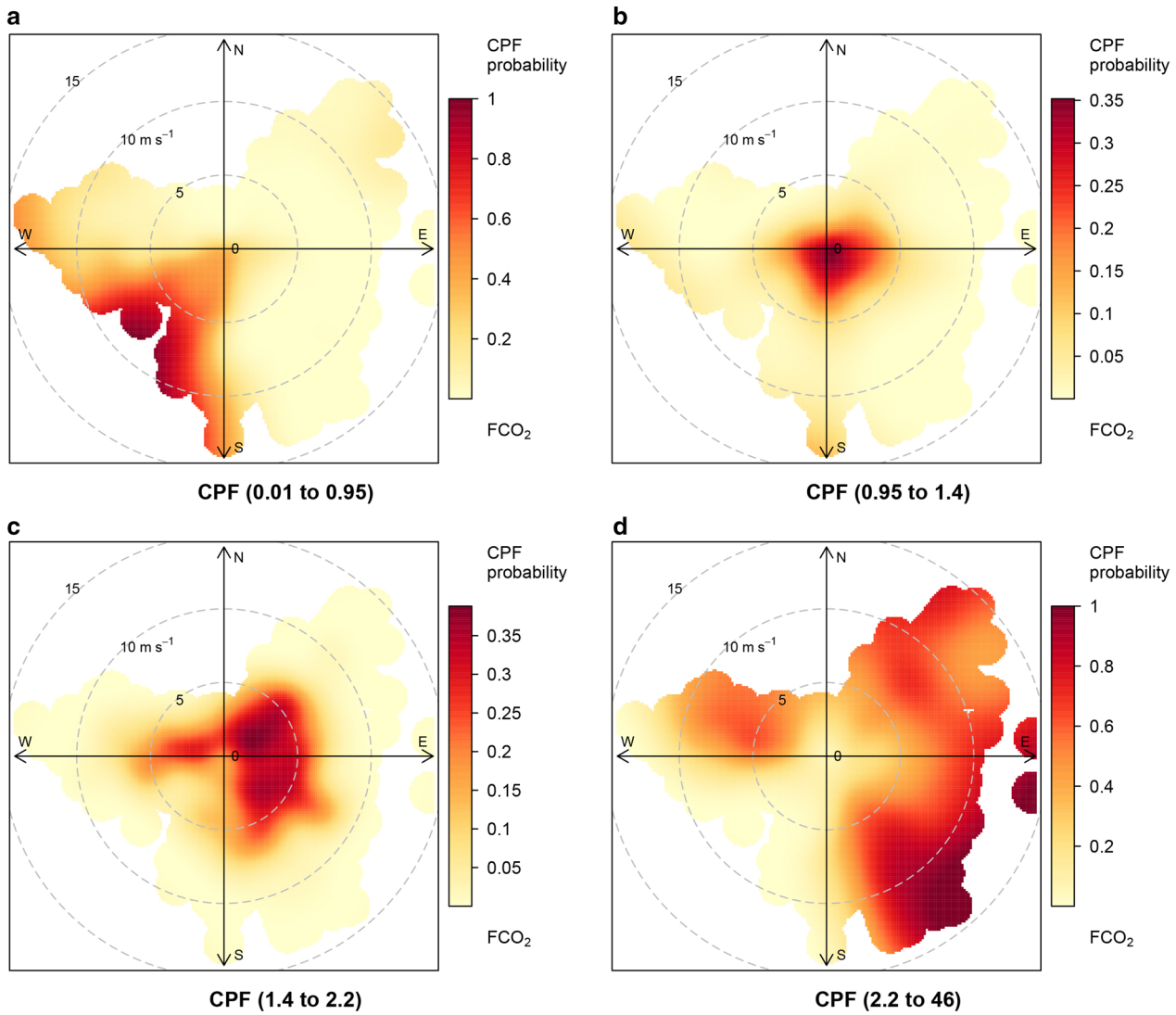

Fig. 6 Polar plots of conditional probabilities of soil CO_2 flux against wind speed and direction. Soil CO_2 fluxes are classified into the **a** first, **b** second, **c** third, and **d** fourth quartiles

recorded with higher wind speeds (Fig. 6c, d). These characteristics have been explained by the Venturi effect due to a local terrain condition around the station (Carapezza et al. 2009). This idea is suitable for our results because the station stood on layered lava flows and tuff (Ono and Watanabe 1985), and thus, strong winds could penetrate the subsurface of the ground.

To identify the periodicity affecting soil CO_2 flux signals, we applied spectral analysis of the data on soil CO_2 flux and environmental parameters using the Lomb–Scargle method (Ruf 1999). This method can obtain periodograms from unevenly spaced time series data. The acquired periodograms of soil CO_2 flux and environmental parameters are shown in Fig. 7. As shown in Fig. 7a, the soil CO_2 flux had semidiurnal (period = 12 h, frequency = 0.083 cph) and diurnal (period = 24 h, frequency = 0.042 cph) peaks, and the semidiurnal peak was stronger than the diurnal peak. A shown in Fig. 7b–i, semidiurnal peaks were observed for air temperature, air relative humidity, barometric pressure, and wind direction, and diurnal peaks were observed for air temperature, air relative humidity, wind speed, wind direction, and precipitation. Moderate and weak diurnal peaks were also observed for soil temperature and soil humidity, respectively. Comparing the amplitude of these two peaks for soil CO_2 flux with those for environmental parameters, the influences of environmental parameters with semidiurnal

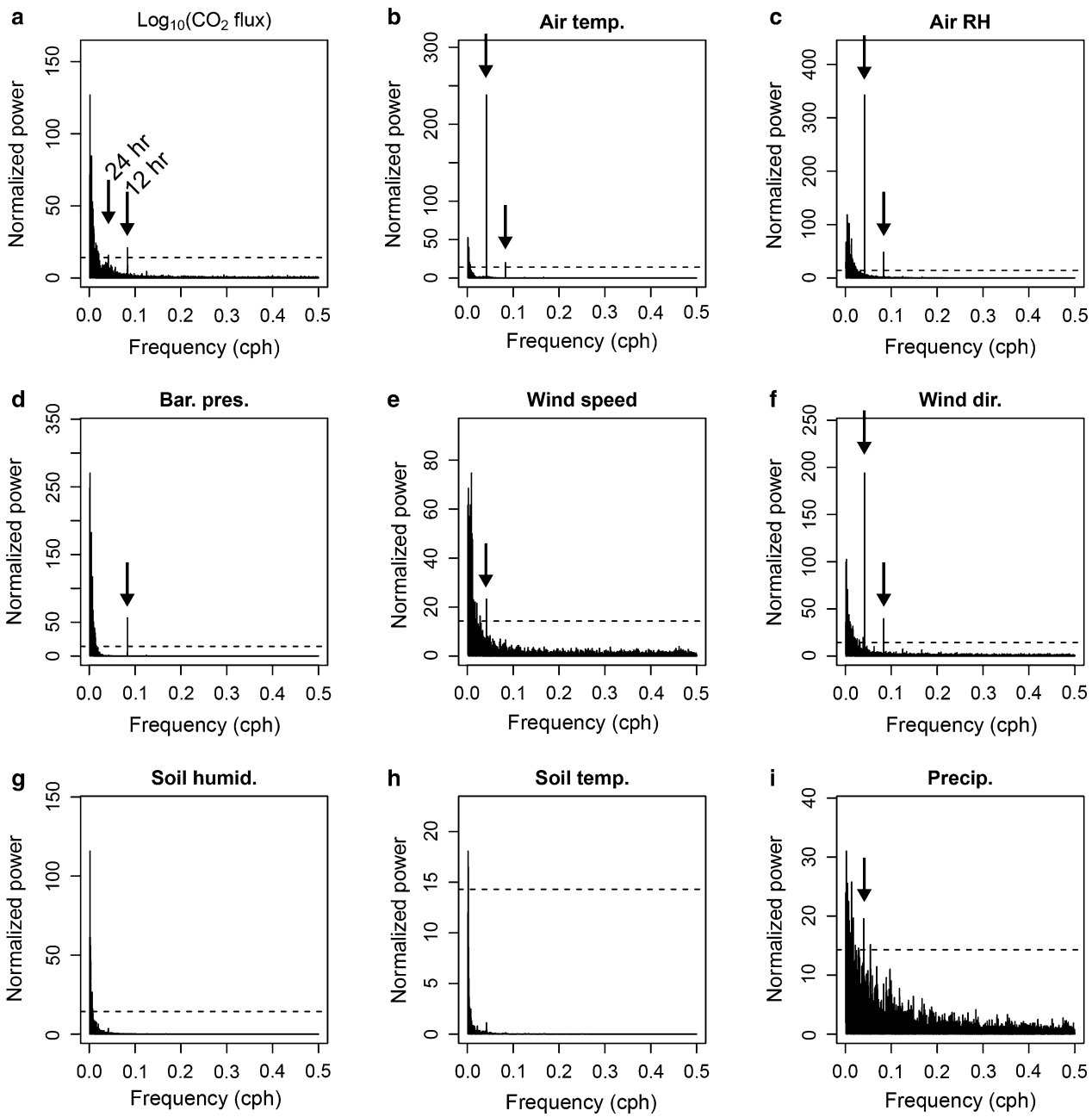

Fig. 7 Lomb–Scargle periodograms of **a** soil CO_2 flux, **b** air temperature, **c** air relative humidity, **d** barometric pressure, **e** wind speed, **f** wind direction, **g** soil humidity, **h** soil temperature, and **i** precipitation. The dotted line in each periodogram corresponds to the level where the probability equals 0.01. The periodogram from 0.001 cph (period = 42 days) to 0.5 cph (2 h) is plotted. The arrows indicate significant diurnal and semidiurnal peaks

peaks were stronger than those with diurnal peaks (e.g., barometric pressure). The presence of diurnal and semidiurnal peaks in the time series of soil CO_2 flux was consistent with the results reported in previous studies (Viveiros et al. 2014; Laiolo et al. 2016), but the magnitude of the amplitudes of these two peaks in our results (semidiurnal peak > diurnal peak) was different from that of previous studies (diurnal peak > semidiurnal peak). This difference in the amplitude relationship between the two peaks was likely related to a different set of environmental parameters influencing the soil CO_2 flux in our case.

Multiple linear regression analysis

Based on the statistical signatures mentioned above, the time series of soil CO_2 flux was likely influenced by environmental parameters. To clarify the influences of environmental parameters on soil CO_2 flux and to remove their contributions from the time series of soil CO_2 flux, a multivariate analysis using the MLR method was applied to the time series of our data set. The detailed procedures of the MLR analysis followed those of Viveiros et al. (2008) and Laiolo et al. (2016). A regression model was developed for the time series in 2017 when the volcanic activity was calm. The logarithmic soil CO_2 flux was considered the dependent variable because soil CO_2 flux showed rough lognormal distributions (Fig. 5). The environmental parameters were treated as the independent variables following the methods of Viveiros et al. (2008). As both the dependent and independent variables, daily average values were used in the model development following the method of Laiolo et al. (2016). Among the environmental parameters, wind direction was not included in the model development because its mathematical treatment in the linear regression analysis was difficult. To determine the regression model, a stepwise method was applied using the *lm* function in the R programming environment (https://www.r-project.org/). In the procedure, all the independent variables were first tested, and then only the significant ones were used in the regression model. The threshold for significant variables was determined to be a 1% increase in the adjusted R^2 value following the methods of Viveiros et al. (2008).

The obtained regression model for the MLR analysis is summarized in Table 3. The model shows that wind speed, barometric pressure, air temperature, soil temperature, and soil humidity were key variables that could explain 50.9% of the variations in soil CO_2 flux in 2017. Based on the increases in adjusted R^2 values (Table 3), wind speed was the most influencing variable on the soil CO_2 flux variations observed in the present study.

The regression model yielded predicted variations in the soil CO_2 flux influenced by environmental parameters. The modeled variations are presented in Fig. 8b, and the observed time series is shown in Fig. 8a. Although the regression model was only able to explain 30.5% of the observed changes during the whole period, many peaks in the modeled values seemed to coincide with those of the observed values not only in the model development period, but also in the whole observation period (Fig. 8b). Residuals were calculated as the difference between the observed soil CO_2 flux and the modeled soil CO_2 flux (Fig. 8c). These values included the influence of variables that were excluded from the model but may also have represented changes due to processes of the volcanic system (Viveiros et al. 2008). Therefore, the baseline trend in the residuals (i.e., low-pass-filtered time series of the residuals) may have reflected the influences of both the excluded variables and the volcanic processes. In Fig. 8c, the time series of the daily average of the residuals (red line) did not deviate significantly from the zero line (dotted line), except for during some periods. Variations during these periods are discussed in the Discussion section.

Discussion

Based on the MLR analysis, 30.5% of the variations in soil CO_2 flux were explained by environmental parameters (wind speed, barometric pressure, air temperature, soil temperature, and soil humidity). In some periods, the residuals of the soil CO_2 flux deviated from the baseline, as shown in Fig. 8c. To emphasize the anomalous values of the residuals, standardized values of the daily average of the residuals are plotted in Fig. 9a. The anomalous values of greater than 2σ are colored with red.

In Fig. 9a, the anomalies of the standardized residuals can be separated into five periods, namely anomalies A1–A5. Anomalies A1–A4 were positive values, which meant that the observed values were higher than the modeled values. Anomaly A5 was a negative value, which

Table 3 Summary of the multiple linear regression analysis for time series in 2017

Independent variable	Coefficient *B*	Standard error of *B*	*t* test	Significance[a] of *t* test	Increase in adjusted R^2
Intercept	9.724	0.408	23.85	< 0.001	
Wind speed	0.0799	0.0015	52.25	< 0.001	0.334
Barometric pressure	− 0.0107	0.0005	− 23.37	< 0.001	0.065
Air temperature	− 0.0294	0.0008	− 34.74	< 0.001	0.012
Soil temperature	0.0304	0.0009	32.88	< 0.001	0.073
Soil humidity	− 0.0133	0.0008	− 16.58	< 0.001	0.025
Adjusted R^2					0.509

[a] Statistical significance of the correlation between each independent variable and dependent variable

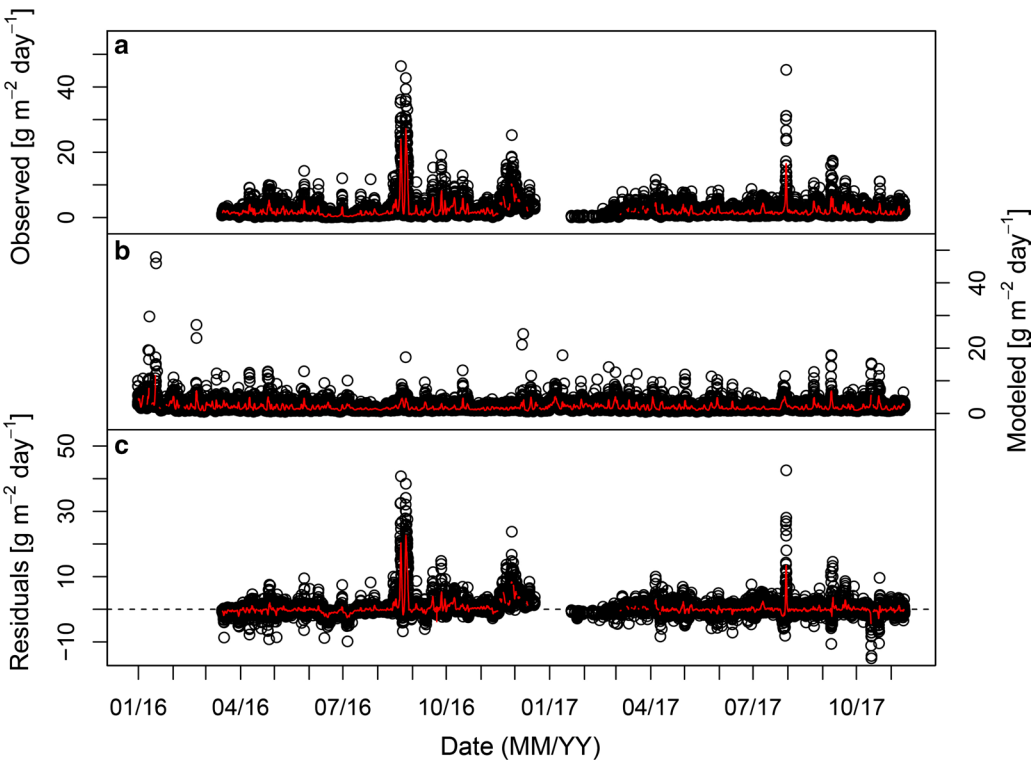

Fig. 8 **a** Observed and **b** modeled time series of soil CO_2 flux and **c** residuals of soil CO_2 flux. The red line shows the daily average values of the data. The dotted line corresponds to the zero level of the residuals

indicated that the model overestimated the influence of the environmental parameters for the corresponding period. In Fig. 9b, the time series of the daily average of the environmental parameters that were included in the model are shown. Comparing Fig. 9a and b, anomalies A1–A5 frequently corresponded to variations in the environmental parameters. For example, the decreases in barometric pressure coincided with the peaks of the anomalies of the residuals for anomalies A1, A4, and A5. The increases in wind speed were simultaneously observed with the anomaly peaks for anomalies A1, A2, A4, and A5. Variations in air temperature, soil temperature, and soil humidity sometimes coincided with the anomaly peaks. Among the environmental parameters in the model, wind speed and barometric pressure were the most effective parameters when viewed in light of their coefficients of the model and their numbers of digits (Table 3). Thus, we compared anomalies A1–A5 with the time series of wind speed and barometric pressure as well as with the volcanic activities.

Close-ups of the time series of standardized residuals of the soil CO_2 flux are compared with the wind speed and barometric pressure in Fig. 10. By comparing Fig. 10a, d with Fig. 10b, e, respectively, the characteristics of anomalies A1–A5 could be denoted as follows:

Anomaly A1

In the first half of the period of anomalies, the peak followed the variations in barometric pressure and slightly corresponded with the variations in wind speed. The peak in the first half of the period was mainly observed in westerly wind conditions. On the other hand, in the second half of the period of anomalies, the peak followed the variations in wind speed but did not coincide with the decrease in barometric pressure. In this period, the wind was almost easterly–southerly.

Anomaly A2

The peak clearly coincided with an increase in wind speed and slightly coincided with a decrease in barometric pressure. The peak was observed with southeasterly wind conditions.

Anomaly A3

The first peak, which was observed with easterly wind conditions, did not coincide with variations in barometric pressure or wind speed. The other peaks mainly coincided with decreases in barometric pressure and increases in wind speed. The wind condition for the

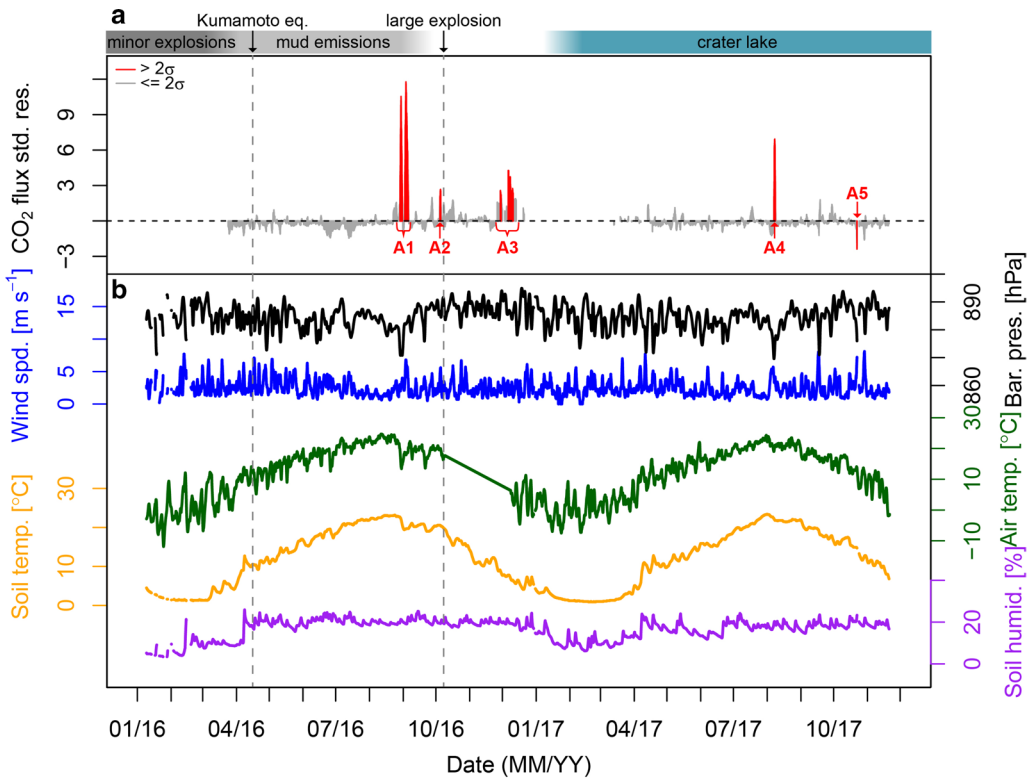

Fig. 9 **a** Time series of the standardized daily average for the residuals of soil CO_2 flux. Only values > 2σ are colored with red. A1–A5 denote the CO_2 flux anomalies discussed in the text. The main volcanic and seismic events are shown in the top of the figure. **b** Time series of the daily average of the environmental parameters that were included in the model. From the top, barometric pressure (black), wind speed (blue), air temperature (green), soil temperature (orange), and soil humidity (purple) are shown

latter peaks was mixed of easterly and westerly winds, but the main direction was from west to southwest.

Anomaly A4

The peak with rotating wind conditions from east to west coincided with a decrease in barometric pressure, but an increase in wind speed was not significant.

Anomaly A5

This was the only negative anomaly. The peak corresponded to both a decrease in barometric pressure and an increase in wind speed. The wind condition was easterly.

Summarizing the characteristics of anomalies A1–A5, the peaks of the anomalies almost coincided with an increase in wind speed and/or a decrease in barometric pressure in varying degrees, except for the first peak of anomaly A3. All the anomalies observed during westerly wind conditions (Fig. 10a, d) coincided with decreases in barometric pressure, and the anomalies during easterly winds coincided with increases in wind speed. In the former case, even though the station may have been influenced by air perturbation in the ground as discussed in the Results section, the large positive anomalies coincided with decreases in barometric pressure. This likely indicated that a decrease in barometric pressure increased the pressure gradient of the ground, and the increase in the pressure gradient enhanced the viscous gas flux (Rogie et al. 2001; Granieri et al. 2003). The latter case could be explained by the Venturi effect due to a local terrain condition around the station (Carapezza et al. 2009). When the influences of both cases contributed to soil CO_2 flux simultaneously (e.g., anomaly A5), our model overestimated their influences. The model should be refined by accumulating longer-term data at this station.

In anomaly A3, the first peak did not coincide with variations in wind speed or barometric pressure. The other peaks in anomaly A3 were observed simultaneously with decreases in barometric pressure and increases in wind speed, but the ranges of the variations were smaller than those of the other anomalies. These peaks occurred with the decreasing trends in air temperature and soil temperature with almost constant soil humidity (Fig. 9). Although the air temperature data were missing due to the malfunctioning of the station, these decreasing trends

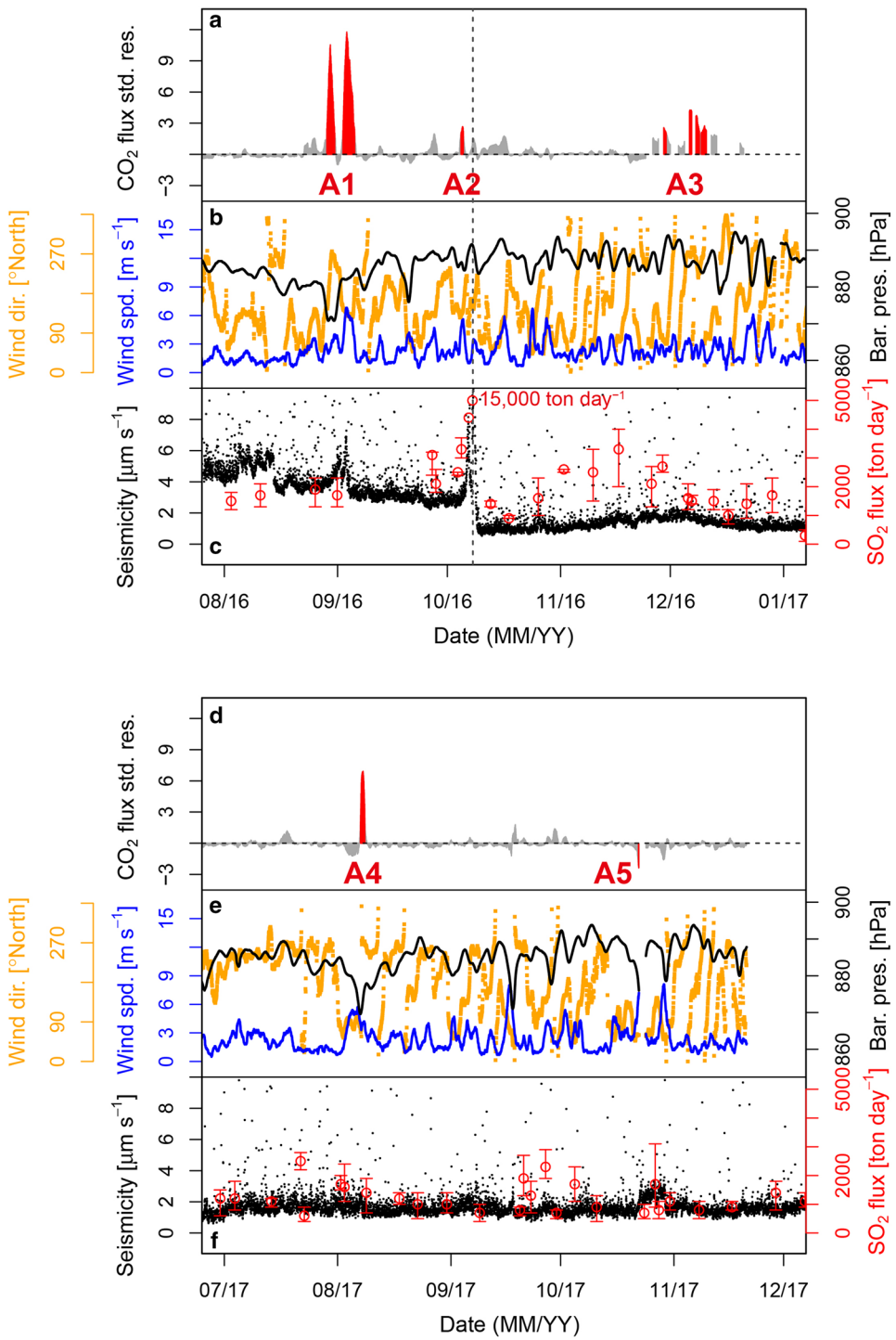

Fig. 10 Time series of **a** the standardized daily average for the residuals of soil CO_2 flux; **b** daily average for wind speed (blue line), wind direction (orange dot), and barometric pressure (black line); and **c** 30 min maximum seismic amplitude (black dot) and plume SO_2 flux (red circle) for the period including anomalies A1–A3. The colors in **a** are the same as those in Fig. 9a. The vertical dashed line in **a**–**c** corresponds to the timing of the 8 October 2016 eruption. The seismic amplitude is recorded at Sunasenri station of Kyoto University, which is 1.3 km S of the active crater, and is filtered at the frequency of 2 Hz. The plume SO_2 flux is from monthly reports by the Japan Meteorological Agency (available at http://www.data.jma.go.jp/svd/vois/data/tokyo/STOCK/monthly_v-act_doc/monthly_vact_vol.php?id=503). **d**–**f** The same time series as a–c for the period including anomalies A4 and A5

in air temperature and soil temperature could have contributed to the increase in soil CO_2 flux based on the correlation coefficients in Table 2. Therefore, anomaly A3 was possibly attributed to the variations in air temperature and soil temperature. Note that the decreasing trends in both values were also observed during October–November 2017, but there were no anomalies during this season (Fig. 9). It is important to carefully check the influences of environmental parameters on soil CO_2 flux even after the procedures of multivariate analysis have been applied to the data.

After careful statistical treatments of the soil CO_2 flux data with the environmental parameters, we compared anomaly A3 to the volcanic activities. The time-averaged seismic amplitude (30 min window and filtered at 2 Hz) and plume SO_2 flux are shown in Fig. 10c. Anomaly A3 was observed approximately one and a half month after the 8 October 2016 eruption and continued for approximately two weeks. The duration of the anomaly was longer than that of the other anomalies. In this period, the seismic amplitude slightly increased, and a peak in the SO_2 flux was also recorded. A previous study revealed that the continuous tremor recorded at Aso volcano was excited in association with the migration of volcanic gas and its interaction with an aquifer under the crater (Takagi et al. 2009). Simultaneously with the increases in the seismic amplitude and SO_2 flux, Cigolini et al. (2018) reported that the thermal signature of the fumarolic area (Fig. 1) was intensified based on satellite and ground-based observations. These data indicated that the magmatic gas from depth was supplied to the hydrothermal system at a higher rate. The simultaneous increases in soil CO_2 flux, continuous tremors, and plume SO_2 fluxes possibly indicated that, during this period, magmatic CO_2 ascended to the station from the hydrothermal system or directly from the conduit. The pathway of the ascending CO_2 remains unclear; thus, we need to conduct further studies on the spatial distribution of soil CO_2 flux, including in this area.

Conclusions

Unrest episodes have occurred at the Nakadake cone of Aso volcano since 2013. The size of the crater lake started to decrease in April 2013, and the crater lake disappeared in July 2014. Following some minor eruptions during this period, magmatic eruptions (intermittent ash emissions and Strombolian eruptions) occurred between November 2014 and May 2015. After these events, the crater lake recovered and large phreatomagmatic eruptions occurred on 14 September 2015, 23 October 2015, and 8 October 2016. The crater lake fully recovered in April 2017 and has remained until the present (December 2018).

Following the unrest episodes, we conducted continuous monitoring of soil CO_2 flux from January 2016 to November 2017 at 1 km southwest of the active crater of Aso volcano using an automated accumulation chamber system. This location was selected because the volcano was very active during the installation, and accessing the summit area during the automated measurements posed a high risk. The results between January 2016 and November 2017 showed that the temporal variations in soil CO_2 flux at our station were highly influenced by environmental parameters. Statistical treatments on the data of soil CO_2 flux and environmental parameters provided good spatial correlations between soil CO_2 flux and wind speed and wind direction. The variations due to environmental parameters were removed from the time series of soil CO_2 flux by MLR analysis. The obtained model explained 30.5% of the variations in soil CO_2 flux in the whole observation period.

In the time series of residuals between those of the observed and the modeled soil CO_2 fluxes, we detected some anomalies (anomalies A1–A5). However, the peaks of the anomalies almost coincided with increases in wind speed and/or decreases in barometric pressure in varying degrees, except for anomaly A3. The anomalies simultaneously observed with these changes in wind speed and/or barometric pressure could be explained by an increase in viscous gas flux in the ground due to the Venturi effect or an increase in pressure gradient in the ground. Anomaly A3 has also been explained by decreases in air temperature and soil temperature. However, these environmental parameters could not explain the CO_2 flux anomaly completely considering its timing and duration, and simultaneous increases in soil CO_2 flux, continuous tremors, and plume SO_2 fluxes in this period possibly indicated that magmatic CO_2 ascended to the station. Careful statistical treatments of the soil CO_2 flux data with the environmental parameters will contribute to developing an effective model to explain soil CO_2 flux variations and to validate the influence of volcanic activity on the observed soil CO_2 flux. Even in the case of a wet volcano with a developed hydrothermal system like Aso volcano, soil CO_2 flux measurement has the potential to detect the migration of magmatic gases from depth.

Additional file

Additional file 1. Detailed information on the continuous monitoring of soil CO_2 flux and supplementary figures and tables. **Figure S1.** A typical slope of an increase of CO_2 concentrations in the accumulation chamber measured at the station. **Figure S2.** Correlation plots of air temperature, precipitation, and air relative humidity between the soil CO_2 flux station

and the weather station. **Figure S3.** A histogram of soil CO_2 flux and correlation plots of soil CO_2 flux to each environmental parameter. **Table S1.** Technical characteristics of the soil CO_2 flux station.

Abbreviations

asl: above sea level; cph: count per hour; JMA: Japan Meteorological Agency; MLR: multiple linear regression.

Authors' contributions

TM, YM, and TO coordinated the project. MM, TM, and AY performed the observation setup. MM performed the analysis of the CO_2 flux and the environmental data and drafted the manuscript. MM, TM, and AY contributed to the interpretation of the data. TO performed the analysis of the seismic data. All authors read and approved the final manuscript.

Author details

[1] Geological Survey of Japan, National Institute of Advanced Industrial Science and Technology, Central 7, Higashi 1-1-1, Tsukuba, Ibaraki 305-8567, Japan. [2] Geochemical Research Center, Graduate School of Science, The University of Tokyo, Hongo 7-3-1, Bunkyo-ku, Tokyo 113-0033, Japan. [3] Aso Volcanological Laboratory, Institute for Geothermal Sciences, Kyoto University, Sakanashi 3028, Ichinomiya-machi, Aso, Kumamoto 869-2611, Japan. [4] Earthquake Research Institute, The University of Tokyo, Yayoi 1-1-1, Bunkyo-ku, Tokyo 113-0032, Japan.

Acknowledgements

We thank Drs. H. Shinohara and T. Kagiyama for their valuable discussions. We are grateful to Drs. C. Cigolini and M. Laiolo and the anonymous reviewers for their insightful comments that greatly improved the manuscript. Figure 6 is generated using the *openair* package (Carslaw and Ropkins 2012; Carslaw 2015) of the R programming environment (https://www.r-project.org/). We would like to thank Editage (www.editage.jp) for English language editing.

Availability of data and materials

The datasets used in this study are available from the corresponding author on reasonable request.

Competing interests

The authors declare that they have no competing interests.

Funding

This study was supported by the Ministry of Education, Culture, Sports, Science and Technology (MEXT) of Japan, under its Earthquake and Volcano Hazards Observation and Research Program.

Publisher's Note

Received: 31 August 2018 Accepted: 21 December 2018
Published online: 07 January 2019

References

Allard P, Carbonnelle J, Dajlevic D, Le Bronec J, Morel P, Robe MC, Maurenas JM, Faivre-Pierret R, Martin D, Sabroux JC, Zettwoog P (1991) Eruptive and diffuse emissions of CO_2 from Mount Etna. Nature 351:387–391. https://doi.org/10.1038/351387a0

Badalamenti B, Bruno N, Caltabiano T, Di Gangi F, Giammanco S, Salerno G (2004) Continuous soil CO_2 and discrete plume SO_2 measurements at Mt. Etna (Italy) during 1997–2000: a contribution to volcano monitoring. Bull Volcanol 66:80–89. https://doi.org/10.1007/s00445-003-0305-y

Baubron JC, Allard P, Toutain JP (1990) Diffuse volcanic emissions of carbon dioxide from Vulcano Island, Italy. Nature 344:51–53. https://doi.org/10.1038/344051a0

Boudoire G, Di Muro A, Liuzzo M, Ferrazzini V, Peltier A, Gurrieri S, Michon L, Giudice G, Kowalski P, Boissier P (2017) New perspectives on volcano monitoring in a tropical environment: continuous measurements of soil CO_2 flux at Piton de la Fournaise (La Réunion Island, France). Geophys Res Lett 44:8244–8253. https://doi.org/10.1002/2017GL074237

Carapezza ML, Inguaggiato S, Brusca L, Longo M (2004) Geochemical precursors of the activity of an open-conduit volcano: the Stromboli 2002–2003 eruptive events. Geophys Res Lett 31:L07620. https://doi.org/10.1029/2004GL019614

Carapezza ML, Ricci T, Ranaldi M, Tarchini L (2009) Active degassing structures of Stromboli and variations in diffuse CO_2 output related to the volcanic activity. J Volcanol Geotherm Res 182:231–245. https://doi.org/10.1016/j.jvolgeores.2008.08.006

Cardellini C, Chiodini G, Frondini F, Avino R, Bagnato E, Caliro S, Lelli M, Rosiello A (2017) Monitoring diffuse volcanic degassing during volcanic unrests: the case of Campi Flegrei (Italy). Sci Rep 7:6757. https://doi.org/10.1038/s41598-017-06941-2

Carslaw DC (2015) The openair manual—open-source tools for analysing air pollution data. Manual for version 1.1–4, King's College London. http://www.openair-project.org

Carslaw DC, Ropkins K (2012) openair—an R package for air quality data analysis. Environ Modell Softw 27–28:52–61. https://doi.org/10.1016/j.envsoft.2011.09.008

Chiodini G, Cioni R, Guidi M, Raco B, Marini L (1998) Soil CO_2 flux measurements in volcanic and geothermal areas. Appl Geochem 13:543–552. https://doi.org/10.1016/S0883-2927(97)00076-0

Chiodini G, Caliro S, Cardellini C, Avino R, Granieri D, Schmidt A (2008) Carbon isotopic composition of soil CO_2 efflux, a powerful method to discriminate different sources feeding soil CO_2 degassing in volcanic-hydrothermal areas. Earth Planet Sci Lett 274:372–379. https://doi.org/10.1016/j.epsl.2008.07.051

Cigolini C, Poggi P, Ripepe M, Laiolo M, Ciamberlini C, Delle Donne D, Ulivieri G, Coppola D, Lacanna G, Marchetti E, Piscopo D, Genco R (2009) Radon surveys and real-time monitoring at Stromboli volcano: influence of soil temperature, atmospheric pressure and tidal forces on ^{222}Rn degassing. J Volcanol Geotherm Res 184:381–388. https://doi.org/10.1016/j.jvolgeores.2009.04.019

Cigolini C, Coppola D, Yokoo A, Laiolo M (2018) The thermal signature of Aso Volcano during unrest episodes detected from space and ground-based measurements. Earth Planets Space 70:67. https://doi.org/10.1186/s40623-018-0831-7

Dionis SM, Pérez NM, Hernández PA, Melián G, Rodríguez F, Padrón E, Sumino H, Barrancos J, Padilla GD, Fernandes P, Bandomo Z, Silva S, Pereira JM, Semedo H, Cabral J (2015) Diffuse CO_2 degassing and volcanic activity at Cape Verde islands, West Africa. Earth Planets Space 67:48. https://doi.org/10.1186/s40623-015-0219-x

Granieri D, Chiodini G, Marzocchi W, Avino R (2003) Continuous monitoring of CO_2 soil diffuse degassing at Phlegraean Fields (Italy): influence of environmental and volcanic parameters. Earth Planet Sci Lett 212:167–179. https://doi.org/10.1016/S0012-821X(03)00232-2

Hernández PA, Notsu K, Salazar JML, Mori T, Natale G, Okada H, Virgili G, Shimoike Y, Sato M, Pérez NM (2001) Carbon dioxide degassing by advective flow from Usu volcano, Japan. Science 292:83–86. https://doi.org/10.1126/science.1058450

Ichimura M, Yokoo A, Kagiyama T, Yoshikawa S, Inoue H (2018) Temporal variation in source location of continuous tremors before ash–gas emissions in January 2014 at Aso volcano, Japan. Earth Planets Space 70:125. https://doi.org/10.1186/s40623-018-0895-4

Ishii K, Hayashi Y, Shimbori T (2018) Using Himawari-8, estimation of SO_2 cloud altitude at Aso volcano eruption, on October 8, 2016. Earth Planets Space 70:19. https://doi.org/10.1186/s40623-018-0793-9

Japan Meteorological Agency (JMA) (2015) Annual report on volcanic activities of Aso volcano in 2014. http://www.data.jma.go.jp/svd/vois/data/tokyo/STOCK/monthly_v-act_doc/fukuoka/2014y/503_14y.pdf. Accessed 27 Dec 2018 (**in Japanese**)

Japan Meteorological Agency (JMA) (2016) Annual report on volcanic activities of Aso volcano in 2015. http://www.data.jma.go.jp/svd/vois/data/tokyo/STOCK/monthly_v-act_doc/fukuoka/2015y/503_15y.pdf. Accessed 27 Dec 2018 (**in Japanese**)

Japan Meteorological Agency (JMA) (2017) Annual report on volcanic activities of Aso volcano in 2016. http://www.data.jma.go.jp/svd/vois/data/tokyo/STOCK/monthly_v-act_doc/fukuoka/2016y/503_16y.pdf. Accessed 27 Dec 2018 (**in Japanese**)

Laiolo M, Ranaldi M, Tarchini L, Carapezza ML, Coppola D, Ricci T, Cigolini C (2016) The effects of environmental parameters on diffuse degassing at Stromboli volcano: insights from joint monitoring of soil CO_2 flux and radon activity. J Volcanol Geotherm Res 315:65–78. https://doi.org/10.1016/j.jvolgeores.2016.02.004

Lewicki JL, Hilley GE (2014) Multi-scale observations of the variability of magmatic CO_2 emissions, Mammoth Mountain, CA, USA. J Volcanol Geotherm Res 284:1–15. https://doi.org/10.1016/j.jvolgeores.2014.07.011

Lewicki JL, Hilley GE, Tosha T, Aoyagi R, Yamamoto K, Benson SM (2007) Dynamic coupling of volcanic CO_2 flow and wind at the Horseshoe Lake tree kill, Mammoth Mountain, California. Geophys Res Lett 34:L03401. https://doi.org/10.1029/2006GL028848

Liuzzo M, Gurrieri S, Giudice G, Giuffrida G (2013) Ten years of soil CO_2 continuous monitoring on Mt. Etna: exploring the relationship between processes of soil degassing and volcanic activity. Geochem Geophys Geosyst 14:2886–2899. https://doi.org/10.1002/ggge.20196

Melián G, Hernández PA, Padrón E, Pérez NM, Barrancos J, Padilla G, Dionis S, Rodríguez F, Calvo D, Nolasco D (2014) Spatial and temporal variations of diffuse CO_2 degassing at El Hierro volcanic system: relation to the 2011–2012 submarine eruption. J Geophys Res Solid Earth 119:6976–6991. https://doi.org/10.1002/2014JB011013

Miyabuchi Y, Terada A (2009) Subaqueous geothermal activity revealed by lacustrine sediments of the acidic Nakadake crater lake, Aso Volcano, Japan. J Volcanol Geotherm Res 187:140–145. https://doi.org/10.1016/j.jvolgeores.2009.08.001

Miyabuchi Y, Iizuka Y, Hara C, Yokoo A, Ohkura T (2018) The September 14, 2015 phreatomagmatic eruption of Nakadake first crater, Aso Volcano, Japan: eruption sequence inferred from ballistic, pyroclastic density current and fallout deposits. J Volcanol Geotherm Res 351:41–56. https://doi.org/10.1016/j.jvolgeores.2017.12.009

Ohsawa S, Saito T, Yoshikawa S, Mawatari H, Yamada M, Amita K, Takamatsu N, Sudo Y, Kagiyama T (2010) Color change of lake water at the active crater lake of Aso volcano, Yudamari, Japan: Is it in response to change in water quality induced by volcanic activity? Limnology 11:207–215. https://doi.org/10.1007/s10201-009-0304-6

Ono K, Watanabe K (1985) Geological map of Aso volcano 1:50,000. Geological Survey of Japan. https://gbank.gsj.jp/volcano/Act_Vol/aso/index-e.html. Accessed 27 Dec 2018

Parkinson KJ (1981) An improved method for measuring soil respiration in the field. J Appl Ecol 18:221–228. https://doi.org/10.2307/2402491

Pérez NM, Hernández PA, Padrón E, Cartagena R, Olmos R, Barahona F, Melián GV, Salazar P, López DL (2006) Anomalous diffuse CO_2 emission prior to the January 2002 short-term unrest at San Miguel Volcano, El Salvador, Central America. Pure appl Geophys 163:883–896. https://doi.org/10.1007/s00024-006-0050-1

Pérez NM, Padilla GD, Padrón E, Hernández PA, Melián GV, Barrancos J, Dionis S, Nolasco D, Rodríguez F, Calvo D, Hernández Í (2012) Precursory diffuse CO_2 and H_2S emission signatures of the 2011–2012 El Hierro submarine eruption, Canary Islands. Geophys Res Lett 39:L16311. https://doi.org/10.1029/2012GL052410

Rogie JD, Kerrick DM, Sorey ML, Chiodini G, Galloway DL (2001) Dynamics of carbon dioxide emission at Mammoth Mountain, California. Earth Planet Sci Lett 188:535–541. https://doi.org/10.1016/S0012-821X(01)00344-2

Ruf T (1999) The Lomb-Scargle periodogram in biological rhythm research: analysis of incomplete and unequally spaced time-series. Biol Rhythm Res 30:178–201. https://doi.org/10.1076/brhm.30.2.178.1422

Saito M, Matsushima T, Matsuwo N, Shimizu H (2007) Observation of SO_2 and CO_2 fluxes in and around the active crater of Aso Nakadake Volcano. Sci Rep Dept Earth Planet Sci Kyushu Univ 22:51–62. https://doi.org/10.15017/6059 **(in Japanese with English abstract)**

Shinohara H, Yoshikawa S, Miyabuchi Y (2015) Degassing activity of a volcanic crater lake: volcanic plume measurements at the Yudamari crater lake, Aso Volcano, Japan. In: Rouwet D, Christenson B, Tassi F, Vandemeulebrouck J (eds) Volcanic Lakes. Springer, Berlin, pp 201–217. https://doi.org/10.1007/978-3-642-36833-2

Stolper E, Holloway JR (1988) Experimental determination of the solubility of carbon dioxide in molten basalt at low pressure. Earth Planet Sci Lett 87:397–408. https://doi.org/10.1016/0012-821X(88)90004-0

Takagi N, Kaneshima S, Ohkura T, Yamamoto M, Kawakatsu H (2009) Long-term variation of the shallow tremor sources at Aso Volcano from 1999 to 2003. J Volcanol Geotherm Res 184:333–346. https://doi.org/10.1016/j.jvolgeores.2009.04.013

Terada A, Hashimoto T, Kagiyama T (2012) A water flow model of the active crater lake at Aso volcano, Japan: fluctuations of magmatic gas and groundwater fluxes from the underlying hydrothermal system. Bull Volcanol 74:641–655. https://doi.org/10.1007/s00445-011-0550-4

Viveiros F, Ferreira T, Cabral Vieira J, Silva C, Gaspar JL (2008) Environmental influences on soil CO_2 degassing at Furnas and Fogo volcanoes (São Miguel Island, Azores archipelago). J Volcanol Geotherm Res 177:883–893. https://doi.org/10.1016/j.jvolgeores.2008.07.005

Viveiros F, Vandemeulebrouck J, Rinaldi AP, Ferreira T, Silva C, Cruz JV (2014) Periodic behavior of soil CO_2 emissions in diffuse degassing areas of the Azores archipelago: application to seismovolcanic monitoring. J Geophys Res Solid Earth 119:7578–7597. https://doi.org/10.1002/2014JB011118

Werner C, Bergfeld D, Farrar CD, Doukas MP, Kelly PJ, Kern C (2014) Decadal-scale variability of diffuse CO_2 emissions and seismicity revealed from long-term monitoring (1995–2013) at Mammoth Mountain, California, USA. J Volcanol Geotherm Res 289:51–63. https://doi.org/10.1016/j.jvolgeores.2014.10.020

Yagi Y, Okuwaki R, Enescu B, Kasahara A, Miyakawa A, Otsubo M (2016) Rupture process of the 2016 Kumamoto earthquake in relation to the thermal structure around Aso volcano. Earth Planets Space 68:118. https://doi.org/10.1186/s40623-016-0492-3

Yokoo A, Miyabuchi Y (2015) Eruption at the Nakadake 1st crater of Aso volcano started in November 2014. Bull Volcanol Soc Jpn 60:275–278. https://doi.org/10.18940/kazan.60.2_275 **(in Japanese)**